Inactivation of *Ascaris* eggs in water using hydrogen peroxide and a Fenton type nanocatalyst (FeOx/C) synthesized by a novel hybrid production process

Ariadna A. Morales, Rafael Schouwenaars, Heriberto Pfeiffer and Rosa María Ramírez-Zamora

ABSTRACT

Inactivation tests of *Ascaris* eggs (Ae) were performed using hydrogen peroxide and a Fenton type nanocatalyst supported on activated carbon (AC) (FeOx/C). Blank inactivation tests were also carried out using H_2O_2 and H_2O_2/AC as oxidation systems. The FeOx/C nanocatalyst was synthesized through a novel hybrid method developed in this work. The method is based on the incipient impregnation technique, using isopropyl alcohol as dissolvent and chelating agent of the iron salt and the ultrasonic method. The supported nanocatalyst contained 2.61% w/w of total iron and the support 0.2% w/w. Transmission electron microscopy (TEM)–energy dispersive spectrometer (EDS) images permitted verification of the presence of finely dispersed FeOx nanoparticles, with sizes ranging from 19 to 63 nm. SEM–EDS analysis and TEM images also showed good dispersion of iron oxide nanoparticles, most probably maghemite; γ-Fe_2O_3, able to produce hydroperoxyl radical as reported in the literature. The FeOx/C nanocatalyst-H_2O_2 system showed an average Ae inactivation efficiency of 4.46% Ae/mg H_2O_2. This value is significantly higher than the result obtained using the support-H_2O_2 system and H_2O_2 alone and it is also better than data reported for the classical Fenton process (homogeneous phase) with or without UV light.

Key words | helminth, heterogeneous Fenton-like reaction, iron oxides, pathogen, reactive oxygen species

Ariadna A. Morales
Rosa María Ramírez-Zamora (corresponding author)
Instituto de Ingeniería,
Universidad Nacional Autónoma de México, Cd. Universitaria,
Coyoacán 04510,
México D.F.,
Mexico
E-mail: *RRamirezZ@iingen.unam.mx*

Rafael Schouwenaars
Facultad de Ingeniería,
Universidad Nacional Autónoma de México,
Cd. Universitaria,
Coyoacán 04510,
México D.F.,
Mexico

Heriberto Pfeiffer
Instituto de Investigaciones en Materiales,
Universidad Nacional Autónoma de México,
Cd. Universitaria,
Coyoacán 04510,
México D.F.,
Mexico

INTRODUCTION

Wastewater is a valuable resource for agricultural use in regions where water resources are scarce. However, its reuse may pose substantial health risks for the agriculturists and consumers, particularly in developing countries, due to the presence of pathogens in raw wastewater, such as helminth eggs (Scoot 2008). Navarro & Jiménez (2011) have reported a content of 70–3,000 helminth eggs/L (He/L) in municipal wastewater of developing countries, which is significantly higher than the value recommended by the WHO (1989) for agricultural irrigation (<1 He/L). *Ascaris* eggs (Ae) are the manifestation of the most common helminth species (84%) identified in wastewater and sludge (Jiménez 2007). This parasite affects 25–33% of the world population, mainly in developing countries (Africa, Latin America and the Far East) (Jiménez 2007). Ae are recalcitrant to most disinfection processes due to their shell, consisting of four organic layers of 3–4 μm thick which protect the eggs, allowing them to remain viable for a long time even under extreme environmental conditions (Brownell & Nelson 2006).

Nelson & Darby (2001) have investigated the validity of using *A. suum*, which infects pigs instead of *A. lumbricoides*, which infects humans, in inactivation tests. Although small genetic differences exist between them, they concluded that their response to inactivation treatments is sufficiently similar to use the more easily

doi: 10.2166/wh.2013.203

obtained *A. suum* in large quantities. They also indicate that there is no significant difference in terms of their infectivity and inactivation between eggs dissected from the intestines of mature female worms and eggs isolated from feces.

Advanced oxidation processes (AOPs), especially the Fenton's reagent, are one of the most efficient technologies for the inactivation of Ae (Solís-López 2009; Solís-López *et al.* 2012). The inactivation of these parasites using the Fenton's reagent occurs through several reactive oxygen species (ROS), such as superoxide and hydroxyl radicals, produced as a result of the catalytic decomposition of hydrogen peroxide by dissolved iron (II). ROS can degrade the compounds of the protecting layers and consequently reduce the protection of the eggs against aggressive environments. Nonetheless, this process has some disadvantages: it is only efficient in a narrow and highly acid pH range; the catalyst or iron is lost as an acidic sludge with the subsequent economic problems and management of hazardous waste (Garrido-Ramírez *et al.* 2010). The heterogeneous Fenton-like process allows these problems to be overcome by using bulk and supported iron species, at micro and nano size scales. This also permits an efficient operation of the Fenton's reagent at neutral pH (Pignatello *et al.* 2006; Garrido-Ramírez *et al.* 2010). It must be mentioned that nanocatalysts are more efficient than micro catalysts, even without using UV light, due to the fact that their catalytic activity improves with the reduction of particle size since the specific contact area is significantly higher than in the case of micro particles (Garrido-Ramírez *et al.* 2010). The use of supported particles on porous materials permits a higher treatment efficiency of dissolved organic pollutants. This is due to the simultaneous occurrence of efficient oxidation and mechanisms such as adsorption.

Three mechanisms for the catalytic decomposition of H_2O_2 on the surface of iron oxides have been reported in the literature (Lin & Gurol 1998; Andreozzi *et al.* 2002; Kwan & Voelker 2004). The mechanism proposed by Lin & Gurol (1998) seems to be the most accepted in the academic community. These authors present a complete series of reactions which are also consistent with other heterogeneous Fenton-like reaction mechanisms. The role of the catalyst in this mechanism is to form a surface complex with the hydrogen peroxide molecule. Reversible electron transfer from ligand to metal can then be compensated by the release of the free OH-radical in the case of Fe (II) and the HO_2-radical for Fe (III), named either hydroperoxyl radical or perhydroxyl radical, which is the protonated form of the superoxide-radical ($pk_a = 4.8$). For the complete sequence of reactions, including termination reactions, the reader is referred to the original work (Lin & Gurol 1998).

Several methods for producing iron oxide nanoparticles supported on porous materials have been reported: precipitation (Adekunle & Ozoemena 2010; Kralj *et al.* 2010), chemical deposition (Cruzat *et al.* 2011), the thermal decomposition process (González-Arellano *et al.* 2008; Balu *et al.* 2010; Wang *et al.* 2010), the chemical vapor deposition technique (Cordier *et al.* 2010), sol-gel (Moliner-Martínez *et al.* 2011), wet impregnation (Lim *et al.* 2006; Da Silva *et al.* 2010; Park *et al.* 2010; Xu *et al.* 2010; Alam *et al.* 2011; Bonelli *et al.* 2011), incipient impregnation (Choi *et al.* 2007; Quintanilla *et al.* 2008; Lu *et al.* 2010; Tsoncheva *et al.* 2010; Hwang *et al.* 2011), ion-exchange (Sarkar *et al.* 2011), and sonochemical process (Jones *et al.* 2010). Nevertheless, these processes can be very complex, time-consuming, and costly. Thus, investigation into the development of economical production methods is required for the preparation of efficient nanomaterials for use in water treatment.

This work presents the results of Ae inactivation tests in water, using hydrogen peroxide and an iron oxide or a Fenton type nanocatalyst supported on activated carbon (AC) (FeOx/C), which was produced by a novel hybrid synthesis method, with the promise of a high cost–benefit ratio.

METHODS

The experimental methodology was divided into three main stages: preparation trials of the nanocatalyst, characterization of the material and its support, and inactivation experiments of Ae using three oxidation systems (hydrogen peroxide alone, H_2O_2 + support and H_2O_2 + FeOx/C).

Materials and reagents

In the synthesis trials, the nanocatalyst's support was a granular AC of mineral origin (LQ 1000, Carbochem Co.) with

grain sizes ranging from 297 to 590 μm. An alcoholic solution of iron 0.63 M was prepared using $Fe(NO_3)_3 \cdot 9H_2O$ (99%, Merck) and isopropyl alcohol (grade HPLC, Burdick & Jackson), as iron source and solvent, respectively. The $Ti(SO_4)_2$ used for the colorimetric method was prepared in our laboratory by acid digestion of TiO_2 (Degussa) and H_2SO_4 (Merck).

For the inactivation tests, hydrogen peroxide at 30% w/w (J. T. Baker) was used. A stock suspension of Ae was prepared in a 0.5% formalin solution with eggs extracted from the uterus of female worms; this suspension, with 92% of initial viability, was stored at 4 °C prior to use. The initial viability of Ae was determined by two techniques, incubation and staining (De Victorica & Galván 2003). Five tests were performed for both, with the results varying 0.8% between the two techniques. A sodium thiosulfate 0.1 N solution was used as received from Hicel (Mexico) for quenching the oxidation reaction.

Preparation of the supported nanocatalyst (FeOx/C)

The FeOx/C nanocatalyst was synthesized by means of a novel hybrid method developed in the present work (Ramírez Zamora *et al.* 2012). It consists of the incipient impregnation technique, using isopropyl alcohol as dissolvent and chelating agent of the iron salt (Hwang *et al.* 2011), and the ultrasonic method. For the incipient impregnation process, 1.43 mL of an alcoholic 0.63 M iron solution were added to 1.121 g of AC by dripping from a syringe and mixing continuously at the same time for preparing a 4% w/w supported Fe nanocatalyst (Bonelli *et al.* 2011). After this, 30 min of ultrasonic treatment (Bransonic 2510R-MT, 100W and 42 kHz ± 6%) was applied for improving the dispersion of the chelated iron salt; this corresponds to the optimal duration as reported by Nagao *et al.* (2007). Finally, to produce the FeOx nanoparticles, the sample was heated at 85 °C (decomposition temperature of isopropyl alcohol, further referred to as calcination) for 40 min with N_2 as carrier gas (30 cm^3/min) in a multifunction system (RIG-100/ISRI). The exhaust gas was analyzed by mass spectroscopy at 8×10^{-6} torr (Hyden Ltd).

Characterization of materials

The diameter of the iron oxide particles present in AC and FeOx/C nanocatalyst was determined by transmission electron microscopy (TEM) with a JEOL JEM-2010 microscope and the ImageJ® version 1.32 software. The iron oxides in AC and FeOx/C were analyzed by means of X-ray diffraction (XRD). Due to the low XRD detection limit (>3% w/w), it was necessary to produce a second nanocatalyst with 10% w/w Fe (10-FeOx/C) using the same method as described above. AC and 10-FeOx/C were analyzed by XRD using a D5000 (Siemens) diffractometer fitted with a CuKα1 radiation source. The powder patterns were recorded from 2 to 90° with a 0.02° step size. The identification of crystalline phases and minerals was carried out using the database powder diffraction file (PDF-2) of the International Centre for Diffraction Data (ICDD).

The surface area of the materials was determined using N_2 adsorption/desorption isotherms at 77 K with a BelSorp mini II analyzer. Before analysis, samples were heated at 80 °C for 12 h under nitrogen atmosphere for degasification.

The total iron content in AC and FeOx/C was measured by atomic absorption spectroscopy after acid digestion (AAS) using a Spectra AA (Varian) model 220 FS spectrophotometer. Determination of the iron content of AC is important as a reference to determine the amount of Fe incorporated in the support, but also because it may contribute to the hydrogen peroxide decomposition in the heterogeneous Fenton-like reaction, i.e., act as a catalyst by itself.

The morphology and the degree of dispersion of the iron oxides in the support (AC) and FeOx/C nanocatalyst were observed through scanning electron microscopy (SEM) with a Philips XL20 microscope equipped with an EDAX energy dispersive spectrometer (EDS).

Inactivation tests of *Ascaris* eggs

The catalytic activity of the FeOx/C nanocatalyst was indirectly measured by performing inactivation tests of Ae. Additionally, two inactivation tests of Ae (blanks) were carried out using H_2O_2 alone and H_2O_2/AC as oxidation systems. All the experiments were performed using 500 mL of a helminth egg suspension containing 2 Ae/mL at an initial pH of 4 (Solís-López 2009). The optimal hydrogen peroxide dose (28.64 mg/L) reported for the Fenton reaction in homogeneous phase by Solís-López (2009) and

the Fe:H_2O_2 mass ratio (1:10) reported by Palma *et al.* (2003) were used in the inactivation tests performed with FeOx/C. The experimental conditions used for AC and FeOx/C were identical. Samples were homogenized in stirred reactors which were protected from light to avoid the photochemical decomposition of hydrogen peroxide. The hydrogen peroxide concentration was measured using the colorimetric method of Eisenberg (1943) at 460 nm with an average deviation of 0.03 mg per 100 mL. The method is based on spectrophotometric measurements of the absorbance of hydrogen peroxide solutions treated with titanium sulfate reagent. The yellow color produced in the reaction is due to the formation of pertitanic acid. After 58 min, the oxidizing action of the hydrogen peroxide residual and ROS was stopped by adding 0.1 mL of sodium thiosulfate in a 0.1 N solution. Then, three samples of 50 mL were collected and filtered on nitrocellulose membranes (8.0 μm pore). The viability of Ae was determined using the vital staining procedure developed by De Victorica & Galván (2003). The viability and inactivation percentages were calculated with the following equations:

$$\%\ \text{Ae viability} = \frac{\text{viable } \textit{Ascaris} \text{ eggs}}{\text{total } \textit{Ascaris} \text{ eggs}} \times 100 \quad (1)$$

$$\%\ \text{of Ae inactivation} = \frac{(\%\ \text{Ae viability})_{\text{initial}} - (\%\ \text{Ae viability})_{\text{final}}}{(\%\ \text{Ae viability})_{\text{initial}}} \times 100 \quad (2)$$

RESULTS AND DISCUSSION

Preparation of the supported nanocatalyst: iron salt decomposition during nanocatalyst calcination

Quantification of gas emission

The exhaust gas generated during nanocatalyst calcination was used to verify the complete decomposition of nitrate and isopropyl alcohol. Figure 1 shows the mass flow of the exhaust gas measured during the decomposition of the iron salt and isopropyl alcohol (NO, NO_2, CO, CO_2, O_2) in the calcination step of the FeOx/C synthesis. The Fe

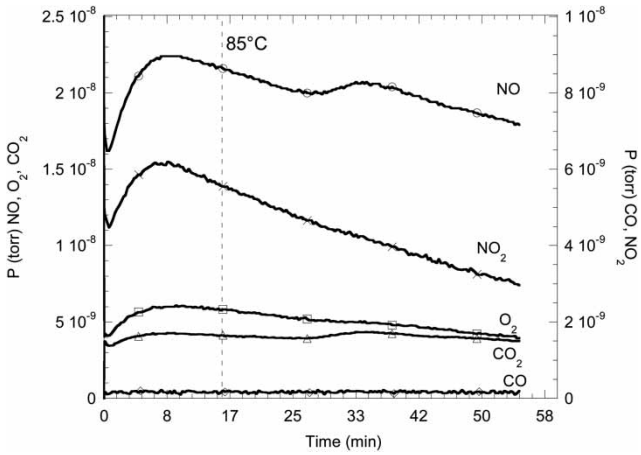

Figure 1 | Mass spectroscopy of the exhaust gases generated during the FeOx/C synthesis.

$(NO_3)_3{\cdot}9H_2O$ decomposition started while heating the sample. The highest emissions of NO, NO_2, and O_2 were observed after 8 min (54 °C). At this point, a CO_2 signal is observed as well. After 10 min of calcination at 85 °C (boiling point of isopropyl alcohol), a NO and CO_2 signal is also observed and continued until the end of the experiment. Throughout the treatment, no CO emissions were detected, suggesting that isopropyl alcohol combustion was complete. The nitrate decomposition occurred according to the following reaction:

$$Fe(NO_3)_3{\bullet}9H_2O_{(s)} \xrightarrow[\Delta]{} NO_{(g)} + NO_{2(g)} + O_{2(g)} + H_2O_{(v)} + FeOx_{(s)} \quad (3)$$

In accordance with our results, at 85 °C, the most probable iron species present in the nanocatalyst is maghemite (γ-Fe_2O_3). This iron oxide species is not effective for producing hydroxyl radicals (as verified by acid salicylic dosimetry in this work); however, perhydroxyl radical ($HO_2{\bullet}$) production by maghemite is possible, as described by Lin & Gurol (1998).

Characterization of materials

Iron content – AAS

The iron content of support (AC) and the synthesized nanocatalyst (FeOx/C) was 0.2% w/w and 2.61% w/w,

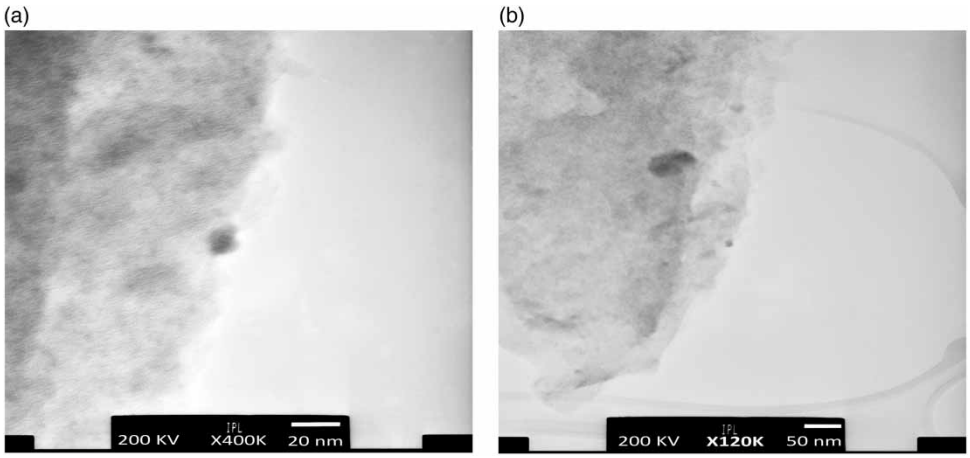

Figure 2 | TEM micrographs of FeOx/C: (a) nanoparticle of 19 nm; (b) nanoparticle of 63 nm.

respectively. The synthesis of the catalyst produces a tenfold increase of the iron content as compared with the support. This value is lower than the theoretical amount (4% w/w) based on the amount of nitrate used, and is similar to the value reported by Bonelli *et al.* (2011). These authors associate this difference to the precipitation of iron oxides in the flask and syringe used in the impregnation process. Based on this result, the nanocatalyst dose showed the same Fe: H_2O_2 mass ratio (1:10) as reported by Palma *et al.* (2003) for the Ae inactivation trial.

Determination of the size and crystalline phase of the iron oxide nanoparticles

The TEM images of FeOx/C (Figure 2) show irregular iron-containing particles (identified by EDS) with diameters ranging from 19 to 63 nm. These values are slightly larger than the ones reported for nanoparticles synthesized by the synthesis methods for nanocatalysts which most closely resemble the actual one (Quintanilla *et al.* 2008; Adekunle & Ozoemena 2010; Lu *et al.* 2010; Wang *et al.* 2010; Cruzat *et al.* 2011); the exception is the work of González-Arellano *et al.* (2008), where larger sizes are reported. The TEM-observations suggest that the supported iron oxides are mainly located on the particle surface.

Not only is the size of the FeOx nanoparticles important, but also their crystalline phase, because the latter plays a determining role in the rate and efficiency of ROS production by the heterogeneous Fenton-like reaction. In the AC sample, only quartz (SiO_2) was identified (JCPDS 046–1045 card). The characteristic reflections of AC between 20–30° and 40–45° (corresponding to the (002) and (001) planes of the graphene stack) were observed. In the 2.1% w/w FeOx/C, it was not possible to detect the diffraction peaks of any iron oxide because its content was below the detection limit of the XRD method. On the other hand, in the 10% w/w Fe catalyst, the XRD pattern suggests the presence of the tetragonal maghemite phase (γ-Fe_2O_3), as evidenced by several small diffraction peaks corresponding to the JCPDS 025–1402 card (Figure 3). This phase has been reported as one of the most active catalysts for the heterogeneous Fenton-like reaction (Wang *et al.* 2008).

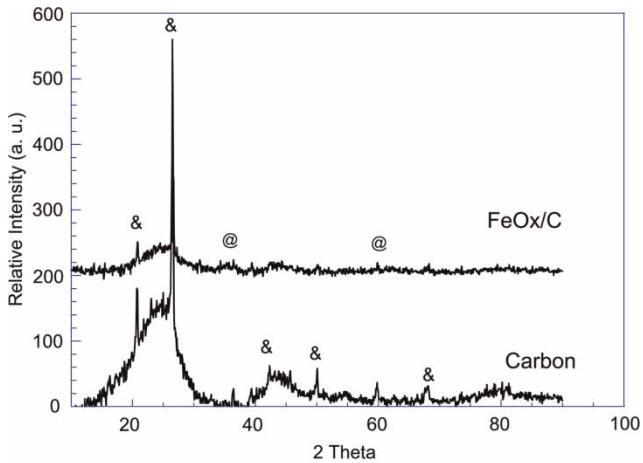

Figure 3 | X-ray diffractogram of support (AC) and catalyst 10-FeOx/C with SiO_2 (&) and maghemite peaks (@).

Morphology and surface chemical composition of the support

Figure 4 shows a series of SEM images of the AC particles and FeOx/C nanocatalyst. It is noted that a large quantity of bright microparticles are already present in the supporting material AC (Figure 4(a)) which are evidently also seen in the FeOx/C nanocatalyst (Figure 4(c)). These are mainly silicates and aluminosilicates, with a considerable fraction consisting of quartz. Some of the mineral particles contain small fractions of Fe as well. A typical close-up of the surface of the supporting material is presented in Figure 4(b). Similar surfaces can easily be found in the FeOx/C material as well.

Not all the particles in the AC sample are identical and different 'surface textures' can be found within the same sample. It is therefore important to compare particles with the same surface appearance when comparing two different samples. The main difference between the starting material

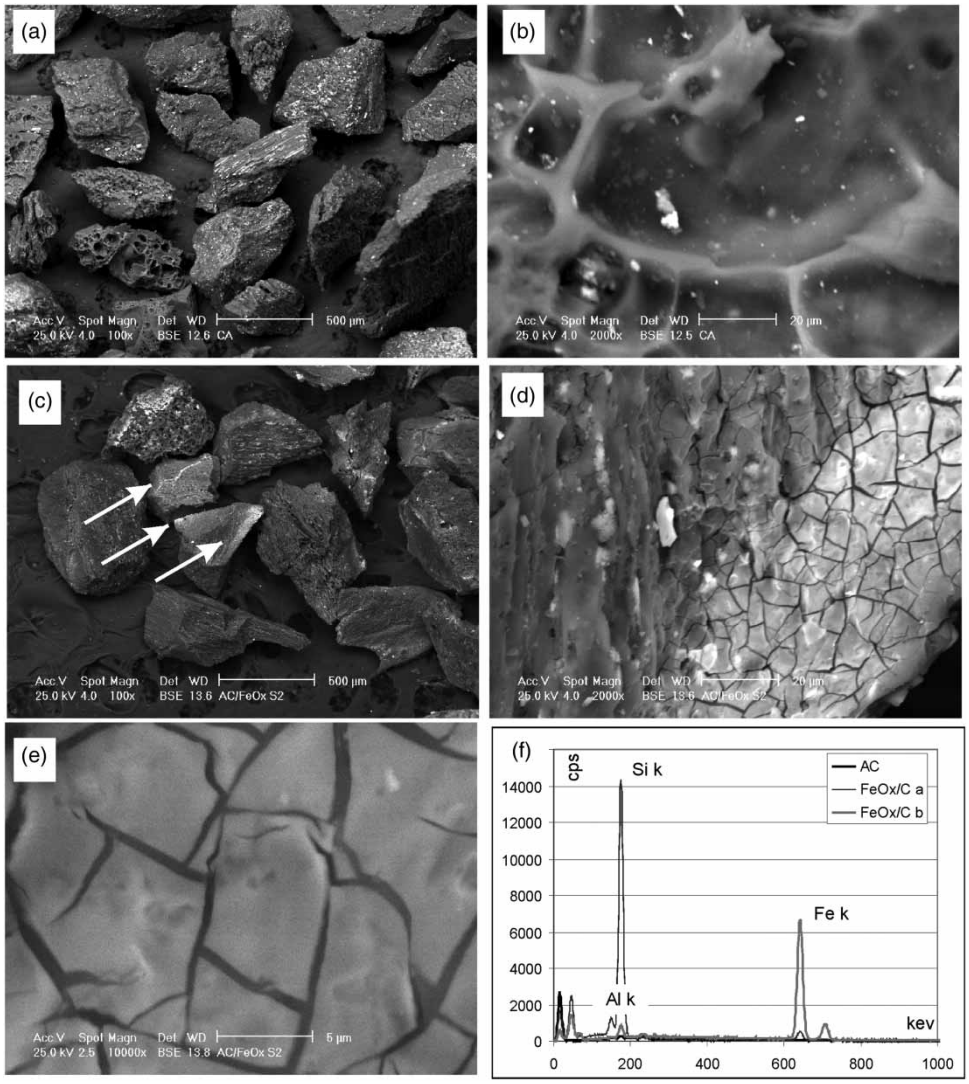

Figure 4 | (a) Supporting material. The white spots in the surface generally are silicate minerals. (b) Detail of the surface of one grain, with a silicate microparticle in the center. (c) FeOx/C. The same white spots as in (a) are seen and are silicate materials. The arrows indicate zones of finely distributed FeOx; it cannot be decided whether these are present on the surface or in the subsurface region by SEM alone. (d) Zone of superficial oxide deposits. (e) Detail of the former; at the amplification given, individual grains cannot be distinguished within the affected zone, indicating that there is either a very fine dispersion of FeOx nanoparticles or a distributed adsorbate of the same material. (f) EDS-spectra of the supporting material (black line), a silicate particle (FeOx/C a) and the iron-rich deposit (FeOx/C b) in (d).

and the supported catalyst is the presence of large, diffuse zones with a brighter tone at the surface and within FeOx/C. A detail of such a zone is shown in Figure 4(d). In Figure 4(e), no individual particles can be observed at high magnifications. The latter image is close to the resolution limit of the SEM, using backscattered electrons. This indicates that FeOx is present either in the form of an adsorbed layer in the carbon or as a fine dispersion of nanoparticles with sizes significantly below the resolution limit of the SEM. On the other hand, TEM results clearly show the presence of the FeOx nanoparticles, the XRD results together with the SEM observations may indicate that at least part of the FeOx is present in the form of an amorphous adsorbate layer on the surface of the support.

Specific surface area – nitrogen adsorption measurements

Figure 5 shows the nitrogen adsorption–desorption isotherms of AC and FeOx/C samples, where both exhibited a typical I type isotherm (Leofanti *et al.* 1998). The adsorption takes place at very low relative pressures because of a strong interaction between pore walls and adsorbate. Although it cannot be excluded that the chemical reaction involved in the synthesis modifies the distribution of the smallest pores, it is more likely that the surface deposition of FeOx as seen in Figures 4(c) and 4(d) closes the access to a significant fraction of the smaller pores.

The average pore diameter was the same (0.2 nm) for both materials. However, the BET surface areas of AC and FeOx/C were different (951.8 and 642.5 m^2/g, respectively). It is expected that the decrease of the nanocatalyst's specific surface area (32.5%) will not negatively influence the production process of ROS because this material shows a significantly (ten times) higher iron content than the support, this latter being the catalyst in the decomposition reaction of hydrogen peroxide. The pore volume of the AC also diminished by 33.7% (from 0.46 cm^3/g to 0.31 m^3/g). These results indicate that FeOx/C nanoparticles partially block the pores of the support, indicating the predominant location of FeOx/C nanoparticles on the outer surface of the supporting material (Tsoncheva *et al.* 2010). This textural characteristic of the sample can facilitate and accelerate the primary catalytic decomposition of hydrogen peroxide into the perhydroxyl radical (HO_2•). The results of dosimetric tests, which are not included in this work, using salicylic acid as a dosimeter, did not show the presence of •OH radical.

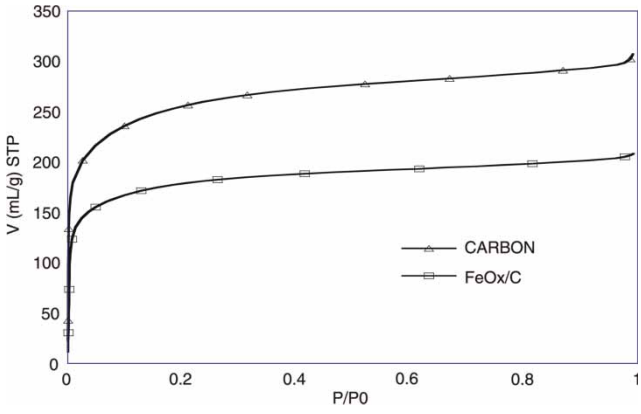

Figure 5 | Nitrogen adsorption isotherms of activated carbon and FeOx/C.

Inactivation tests of *Ascaris* eggs

Table 1 shows the results of the inactivation tests of Ae, which are compared with data reported in the literature for similar processes. When the FeOx/C-H_2O_2 system is compared with the use of hydrogen peroxide alone, the latter has low inactivation efficiency (0.56% Ae/mg H_2O_2). The support-hydrogen peroxide system without iron oxides showed an even lower catalytic activity (0.084% Ae inactivation/mg H_2O_2) as compared with H_2O_2 alone. This result was expected since iron oxides (catalyst) are virtually absent in the support for the perhydroxyl radical (HO_2•) production; Fe is mostly contained in compact alumino-silicates present in the ash fraction of AC and these silicates have no significant catalytic effect on hydrogen peroxide molecules. In the absence of active iron species for the production of these ROS, an oxidation–reduction reaction between AC carbon (reducing agent) and hydrogen peroxide (oxidant) can take place. In fact, AC is often used in water treatment for the elimination of residual oxidants, such as ozone and chlorine (Gopal *et al.* 2007).

Several studies have demonstrated an oxidant effect of HO_2•/O_2• radicals on different types of bacteria through a lipid peroxidation mechanism which produces DNA damage (Termini 2000; Rincon & Pulgarin 2006, 2007a,

Table 1 | Percentages of Ae inactivation for homogeneous and heterogeneous Fenton-like reactions

	Homogeneous Fenton-like reaction Without UV light		With UV light		Solar	Heterogeneous Fenton-like reaction Without UV light
	Ramírez *et al.* (2006a)	Solís-López (2009)	Ramírez *et al.* (2006b)	Solís-López (2009)	Bandala *et al.* (2011)	This work
% of Ae inactivation/mg H_2O_2	3.34	1.01	0.46	1.34	0.18	4.30 ± 0.23
Total Ae (Ae/mL)	2	2	2	2	0.3	2
Doses H_2O_2 (mg/L)	40	28.64	40	21.90	9,520	28.64
Fe/H_2O_2 (w/w)	10	11.24	2	0.07	0.058	0.1
pH	3	3	3	3	3	4
Time (min)	50	58.5	50	32.5	120	58

2007b; Dramou *et al.* 2008; Imlay 2008; Moncayo *et al.* 2008; Maroz *et al.* 2009; Mazille *et al.* 2010; Sciacca *et al.* 2010; Joshi *et al.* 2011; Huang *et al.* 2012; Lanao *et al.* 2012).

According to Table 1, the FeOx/C nanocatalyst showed a significantly higher catalytic activity (4.30 ± 0.23% Ae inactivation/mg H_2O_2) than data reported for various iron salts used in the Fenton's reagent, with similar experimental conditions. The inactivation percentage obtained in this work is between 1.3 and 3.5 times higher than data reported for the homogeneous Fenton-like reaction without UV light (Ramírez *et al.* 2006a; Solís-López 2009) and it was also more efficient than results obtained with UV light assisted photo-Fenton systems (Ramírez *et al.* 2006b; Solís-López 2009) and solar light assisted Fenton reactions (Bandala *et al.* 2011). The reaction time in most of these studies, with the exception of solar Fenton, is similar to the value used in this work. However, the hydrogen peroxide dose in the present work was significantly lower; therefore, the method presented here may present a higher cost–benefit ratio as compared with other Fenton and Fenton-like oxidation systems.

The results of Table 1 indicate that the iron oxide nanoparticles could indeed provide a sufficiently large area of active sites for an efficient H_2O_2 decomposition by the heterogeneous Fenton-like reaction. This can be due to the size and high dispersion of these nanoparticles supported on the AC surface.

An important advantage in the use of the present supported nanocatalyst is that lixiviated iron concentration was very low (0.07 mg/L) and thus no acidic sludge is generated in the process, eliminating the treatment costs of this hazardous waste. Also, this supported nanocatalyst can be recovered by filtration or electromagnetic processes making possible its reuse with a significant cost reduction.

An economic analysis was developed considering the costs for the production of the nanocatalyst and those for the disinfection process (Table 2). For this economic analysis, we considered 4% of inflation rate and 100% of financial leverage with 20% of interest for the nanocatalyst production and 6% of interest for the disinfection process. The disinfection process is self-financed (internal rate of return = zero) in 5 years. Table 2 shows that the cost for wastewater treatment (0.128 USD/m^3) is similar to data (0.18 USD/m^3) reported by EPA (2006) for a drinking water treatment plant with an average flow of 350 mdg. The operational cost can be reduced by further optimizing the production process of the nanocatalyst and the operation parameters of the disinfection process.

Table 2 | Costs of the nanocatalyst production and the disinfection process

	Nanocatalyst production	Disinfection process
Production	342 ton/year	23 m^3/s
Raw materials (USD/day)	$148,089	$182,727
Equipment (USD)	$92,683	$4,615,000
Wages (USD/year)	$488,049	$258,878
Operation and management expenses (USD/year)	$10,569	$273,351
Unit cost	$186,492 USD/ton	$0.128 USD/$m^3$

CONCLUSIONS

A high inactivation rate of Ae (4.46% inactivated Ae/mg H_2O_2) was obtained by using hydrogen peroxide and a Fenton type nanocatalyst. The contribution of the support and H_2O_2 to Ae inactivation was not significant (0.084% Ae inactivation/mg H_2O_2 and 0.56% Ae inactivation/mg H_2O_2, respectively). The FeOx/C inactivation Ae efficiency was higher than other Fenton processes reported in literature up to now.

The nanocatalyst used in the Ae inactivation was prepared through a novel and simple synthesis method developed in this work. This produced well-dispersed iron oxide nanoparticles (most probably maghemite; γ-Fe_2O_3 with sizes of 19–63 nm) supported on AC. Maghemite has been reported as one of the most reactive iron phases for the heterogeneous Fenton-like reaction. The presence of well-dispersed maghemite particles at nano scale can explain the high catalytic activity of the FeOx/C nanocatalyst synthesized in this work.

ACKNOWLEDGEMENTS

The authors are grateful to PhD Gretchen T. Lapidus Lavine and PhD Gustavo Fuentes Zurita from the *Universidad Autónoma Metropolitana – Iztapalapa* for the AA analysis and for the use of the RIG-100/ISRI equipment, respectively. They also thank Ivan Puente Lee from the *Universidad Nacional Autónoma de Mexico* for the TEM analysis. Ariadna A. Morales thanks the *CEP-UNAM* for the PhD grant. The work was supported by CONACYT under grant No. SEP-2004-C01-48097. The authors thank Gustavo Cadena from the *Universidad Nacional Autónoma de Mexico* for the economic analysis.

REFERENCES

Adekunle, A. & Ozoemena, K. 2010 Voltammetric and impedimetric properties of nano-scaled Fe_2O_3 catalyst supported on multi-walled carbon nanotubes: catalytic detection of dopamine. *Int. J. Electrochem. Sci.* **5**, 1726–1742.

Alam, S., Anand, C., Zaidi, S., Siddulu, T., Al-Deyab, S. & Vinu, A. 2011 Iron oxide nanoparticles embedded onto 3D mesochannels of KIT-6 with different pore diameters and their excellent magnetic properties. *Chem. – An Asian J.* **6**, 834–841.

Andreozzi, R., Caprio, V. & Marotta, R. 2002 Oxidation of 3,4-dihydroxybenzoic acid by means of hydrogen peroxide in aqueous goethite slurry. *Water Res.* **36**, 2761–2768.

Balu, A., Pineda, A., Yoshida, K., Campelo, J., Gai, P., Luque, R. & Romero, A. 2010 Fe/Al synergy in Fe_2O_3 nanoparticles supported on porous aluminosilicate materials: excelling activities in oxidation reactions. *Chem. Commun.* **46**, 7825–7827.

Bandala, E., González, L., de la Hoz, F., Pelaez, M., Dionysiou, D., Dunlop, P., Byrne, J. & Sanchez, J. 2011 Application of azo dyes as dosimetric indicators for enhanced photocatalytic solar disinfection (ENPHOSODIS). *J. Photochem. Photobiol. A* **218**, 185–191.

Bonelli, R., Albonetti, S., Morandi, V., Ortolani, L., Riccobene, P., Scirè, S. & Zacchini, S. 2011 Design of nano-sized FeOx and Au/FeOx catalysts supported on CeO_2 for total oxidation of VOC. *Appl. Catal. A* **395**, 10–18.

Brownell, S. & Nelson, K. 2006 Inactivation of single-celled *Ascaris suum* eggs by low-pressure UV radiation. *Appl. Environ. Microb.* **72**, 2178–2184.

Choi, H. C., Jung, H. R. & Kim, J. 2007 Alumina-supported iron oxide nanoparticle comprising iron oxide fixed on an alumina support with an organic substance. Korea Patent 100784167.

Cordier, A. G., de Resende, V., Weibel, A., De Grave, E., Peigney, A. & Laurent, C. 2010 Catalytic chemical vapor deposition synthesis of double-walled and few-walled carbon nanotubes by using a MoO3-supported conditioning catalyst to control the formation of iron catalytic particles within an γ-Al1.8Fe0.2O3 self-supported foam. *J. Phys. Chem.* **114**, 19188–19193.

Cruzat, C., Peña, O., Meléndrez, M., Díaz Visurraga, J. & Cárdenas, G. 2011 Synthesis, characterization and properties of magnetic colloids supported on chitosan. *Colloid Polym. Sci.* **289**, 21–31.

Da Silva, D., Skeff, K., Coaquira, J., Araujo, P., Cintra, D., Lima, E., Guilherme, L., Mosiniewicz-Szablewska, E. & Morais, P. 2010 Magnetic characterization of vermiculite-based magnetic nanocomposites. *J. Non-Cryst. Solids* **356**, 2574–2577.

De Victorica, J. & Galván, M. 2003 Preliminary testing of a rapid coupled methodology for quantitation/viability determination of helminth eggs in raw and treated wastewater. *Water Res.* **37**, 1278–1287.

Dramou, B., Shah, V. & Pinto, J. 2008 A kinetic model for microbial decontamination of water based on a modified Fenton reaction. *Energy Environ. Sci.* **1**, 395–402.

EPA 2006 Technology and Cost Document for the Final Ground Water Rule. Available at: http://www.epa.gov/ogwdw/disinfection/gwr/pdfs/support_gwr_cost-technologies.pdf (accessed 8 March 2013).

Garrido-Ramírez, E. G., Theng, B. K. G. & Mora, M. L. 2010 Clays and oxide minerals as catalysts and nanocatalysts in Fenton-like reactions – a review. *Appl. Clay Sci.* **47**, 182–192.

González-Arellano, C., Campelo, J., Macquarrie, D., Marinas, J., Romero, A. & Luque, R. 2008 Efficient microwave oxidation of alcohols using low-loaded supported metallic iron nanoparticles. *Chem. Sus. Chem.* **1**, 746–750.

Gopal, K., Tripathy, S., Bersillon, J. & Dubey, S. 2007 Chlorination byproducts, their toxicodynamics and removal from drinking water. *J. Hazard. Mater.* **140**, 1–6.

Huang, L., Xuan, Y., Koide, Y., Zhiyentayev, T., Tanaka, M. & Hamblin, M. 2012 Type I and type II mechanisms of antimicrobial photodynamic therapy: an *in vitro* study on Gram-negative and Gram-positive bacteria. *Laser. Surg. Med.* **44**, 490–499.

Hwang, W. S., Liu, S.-J., Huang, C.-H. & Huang, C.-K. 2011 Iron complex, manufacturing method thereof and supported iron oxide catalyst constructed thereby. Patent Application US 20110160045A1, United States.

Imlay, J. A. 2008 Cellular defenses against superoxide and hydrogen peroxide. *Annu. Rev. Biochem.* **77**, 755–776.

Jiménez, B. 2007 Helminth ova removal from wastewater for agriculture and aquaculture reuse. *Water Sci. Technol.* **55**, 485–493.

Jones, W., Rangari, V., Hassan, T. & Jeelani, S. 2010 Synthesis and characterization of (Fe_3O_4/MWCNTs)/epoxy nanocomposites. *J. Appl. Polym. Sci.* **116**, 2783–2792.

Joshi, S., Cooper, M., Yost, A., Paff, M., Ercan, U., Fridman, G., Friedman, G., Fridman, A. & Brooks, A. 2011 Nonthermal dielectric-barrier discharge plasma-induced inactivation involves oxidative DNA damage and membrane lipid peroxidation in *Escherichia coli*. *Antimicrob. Agents Chemother.* **55**, 1053–1062.

Kralj, S., Makovec, D., Campelj, S. & Drofenik, M. 2010 Producing ultra-thin silica coatings on iron-oxide nanoparticles to improve their surface reactivity. *J. Magn. Magn. Mater.* **322**, 1847–1853.

Kwan, W. & Voelker, B. 2004 Influence of electrostatics on the oxidation rates of organic compounds in heterogeneous Fenton systems. *Environ. Sci. Technol.* **38**, 3425–3431.

Lanao, M., Ormad, M., Mosteo, R. & Ovelleiro, J. 2012 Inactivation of *Enterococcus* sp. by photolysis and TiO_2 photocatalysis with H_2O_2 in natural water. *Sol. Energy* **86**, 619–625.

Leofanti, G., Padovan, M., Tozzola, G. & Venturelli, B. 1998 Surface area and pore texture of catalysts. *Catal. Today* **41**, 207–219.

Lim, H., Lee, J., Jin, S., Kim, J., Yoon, J. & Hyeon, T. 2006 Highly active heterogeneous Fenton catalyst using iron oxide nanoparticles immobilized in alumina coated mesoporous silica. *Chem. Commun.* **4**, 463–465.

Lin, S. & Gurol, M. 1998 Catalytic decomposition of hydrogen peroxide on iron oxide: kinetics, mechanism and implications. *Environ. Sci. Technol.* **32**, 1417–1423.

Lu, A.-H., Nitz, J., Comotti, M., Weidenthaler, C., Schlichte, K., Lehmann, C., Terasaki, O. & Schüth, F. 2010 Spatially and size selective synthesis of Fe-based nanoparticles on ordered mesoporous supports as highly active and stable catalysts for ammonia decomposition. *J. Am. Chem. Soc.* **132**, 14152–14162.

Maroz, A., Anderson, R. F., Smith, R. A. J. & Murphy, M. P. 2009 Reactivity of ubiquinone and ubiquinol with superoxide and the hydroperoxyl radical: implications for *in vivo* antioxidant activity. *Free Radic. Biol. Med.* **46** (1), 105–109.

Mazille, F., Moncayo-Lasso, A., Spuhler, D., Serra, A., Peral, J., Benítez, N. & Pulgarin, C. 2010 Comparative evaluation of polymer surface functionalization techniques before iron oxide deposition. Activity of the iron oxide-coated polymer films in the photo-assisted degradation of organic pollutants and inactivation of bacteria. *Chem. Eng. J.* **160**, 176–184.

Moliner-Martínez, Y., Ribera, A., Coronado, E. & Campíns-Falcó, P. 2011 Preconcentration of emerging contaminants in environmental water samples by using silica supported Fe_3O_4 magnetic nanoparticles for improving mass detection in capillary liquid chromatography. *J. Chromatogr. A.* **1218**, 2276–2283.

Moncayo-Lasso, A., Torres-Palma, R., Kiwi, J., Benítez, N. & Pulgarin, C. 2008 Bacterial inactivation and organic oxidation via immobilized photo-Fenton reagent on structured silica surfaces. *Appl. Catal. B: Environ.* **84**, 577–583.

Nagao, D., Shimazaki, Y., Saeki, S., Kobayashi, Y. & Konno, M. 2007 Effect of ultrasonic irradiation on carbon-supported Pt-Ru nanoparticles prepared at high metal concentration. *Colloid. Surf. A.* **302**, 623–627.

Navarro, I. & Jiménez, B. 2011 Evaluation of the WHO helminth eggs criteria using a QMRA approach for the safe reuse of wastewater and sludge in developing countries. *Water Sci. Technol.* **63**, 1499–1505.

Nelson, K. & Darby, J. 2001 Inactivation of viable *Ascaris* eggs by reagents during enumeration. *Appl. Environ. Microb.* **67**, 5453–5459.

Palma, L., Ferrantelli, P. & Petrucci, E. 2003 Experimental study of the remediation of atrazine contaminated soils through soil extraction and subsequent peroxidation. *J. Hazard. Mater.* **99**, 265–276.

Park, J., Lee, Y., Khanna, P., Jun, K., Wook, J. & Ho, Y. 2010 Alumina-supported iron oxide nanoparticles as Fischer-Tropsch catalysts: effect of particle size of iron oxide. *J. Mol. Catal. A-Chem.* **323**, 84–90.

Pignatello, J. J., Oliveros, E. & Mackay, A. 2006 Advanced oxidation processes for organic contaminant destruction based on the Fenton reaction and related chemistry. *Crit. Rev. Environ. Sci. Technol.* **36**, 1–84.

Quintanilla, A., Menéndez, N., Tornero, J., Casas, J. & Rodríguez, J. 2008 Surface modification of carbon-supported iron catalyst during the wet air oxidation of phenol: influence on activity, selectivity and stability. *Appl. Catal. B-Environ.* **81**, 105–114.

Ramírez Zamora, R., Galván, M., Rodríguez, A., Espejel, F. & Retama, I. 2006a Evaluación del reactivo de Fenton para reducir el porcentaje de viabilidad de huevos de Helminto (*Ascaris suum*) en medio acuoso. (Fenton reaction evaluation for reducing viability percentage of helminth eggs (*Ascaris suum*) in aqueous environment). XV National Conference of

Health Engineering and Environmental Sciences, Guadalajara México.

Ramírez Zamora, R., Galván, M., Retama, I., Rigas, F. & Duran-Moreno, A. 2006b Viability reduction of parasites (*Ascaris* spp.) in water with photo-Fenton reaction via response surface methodology. *Water Pract. Technol.* **1**, 1–8.

Ramírez Zamora, R., Morales, A. & Schouwenaars, R. 2012 Proceso de Producción de un nanocatalizador tipo Fenton de nanopartículas de óxidos de hierro soportadas en materiales porosos para la oxidación de contaminantes presentes en agua (Production process of a nanocatalyst Fenton-type of iron oxide nanoparticles supported on porous materials for the oxidation of contaminants in water). Patent application MX/a/2012/000450, January 9, 2012, Mexico.

Rincon, A. G. & Pulgarin, C. 2006 Comparative evaluation of Fe^{3+} and TiO_2 photoassisted processes in solar photocatalytic disinfection of water. *Appl. Catal. B: Environ.* **63**, 222–231.

Rincon, A. G. & Pulgarin, C. 2007a Fe^{3+} and TiO_2 solar-light-assisted inactivation of *E. coli* at field scale. Implications in solar disinfection at low temperature of large quantities of water. *Catal. Today* **122**, 128–136.

Rincon, A. G. & Pulgarin, C. 2007b Absence of *E. coli* regrowth after Fe^{3+} and TiO_2 solar photo assisted disinfection of water in CPC solar photoreactor. *Catal. Today* **124**, 204–214.

Sarkar, S., Chatterjee, P., Cumbal, L. & SenGupta, A. 2011 Hybrid ion exchanger supported nanocomposites: sorption and sensing for environmental applications. *Chem. Eng. J.* **166**, 923–931.

Sciacca, F., Rengifo-Herrera, J., Wéthè, J. & Pulgarin, C. 2010 Dramatic enhancement of solar disinfection (SODIS) of wild *Salmonella* sp. in PET bottles by H_2O_2 addition on natural water of Burkina Faso containing dissolved iron. *Chemosphere* **78**, 1186–1191.

Scoot, M. 2008 *Ascaris lumbricoides*: a review of its epidemiology and relationship to other infections. *An. Nestlé* **66**, 7–22.

Solís-López, M. 2009 Inactivation of *Ascaris* Eggs in Water by Fenton with and without UV Light. Master's Thesis, Universidad Nacional Autónoma de México, Mexico. Available at: http://132.248.9.195/ptd2009/junio/0644767/Index.html (accessed 15 October 2012).

Solís-López, M., Durán-Moreno, A., Navarrete-Montesinos, M. & Ramírez-Zamora, R. M. 2012 Assessment of slags as photocatalyst in the solar photo Fenton-like reaction for water disinfection. *IWA Regional Conference on Wastewater Purification & Reuse (WWPR2012)*, Crete, Greece, 20–22 March, 2012.

Termini, J. 2000 Hydroperoxide-induced DNA damage and mutations. *Mutat. Res.* **450**, 107–124.

Tsoncheva, T., Roggenbuck, J., Paneva, D., Dimitrov, M., Mitov, I. & Fröba, M. 2010 Nanosized iron and chromium oxides supported on mesoporous CeO_2 and SBA-15 silica: physicochemical and catalytic study. *Appl. Surf. Sci.* **257**, 523–530.

Wang, X., Liu, C., Li, X., Li, F. & Zhou, S. 2008 Photodegradation of 2-mercaptobenzothiazole in the γ-Fe_2O_3/oxalate suspension under UVA light irradiation. *J. Hazard. Mater.* **153**, 426–433.

Wang, X., Zhao, Z., Qu, J., Wang, Z. & Qiu, J. 2010 Fabrication and characterization of magnetic Fe_3O_4-CNT composites. *J. Phys. Chem. Solids* **71**, 673–676.

WHO 1989 *Health guidelines for the use of wastewater in agriculture and aquaculture*. Report of World Health Organization, Geneva, Switzerland.

Xu, J., Gao, N., Tang, Y., Deng, Y. & Sui, M. 2010 Perchlorate removal using granular activated carbon supported iron compounds: synthesis, characterization and reactivity. *J. Environ. Sci.* **22**, 1807–1813.

First received 29 October 2012; accepted in revised form 29 April 2013. Available online 4 June 2013